Please cite this article in press as: Hu et al., Terbinafine prevents colorectal cancer growth by inducing dNTP starvation and reducing immune suppression, Molecular Therapy (2022), https://doi.org/10.1016/j.ymthe.2022.06.015

Molecular Therapy
Original Article

Terbinafine prevents colorectal cancer growth by inducing dNTP starvation and reducing immune suppression

Li-Peng Hu,[1,7] Wuqing Huang,[2,7] Xu Wang,[3,7] Chunjie Xu,[1,7] Wei-Ting Qin,[1] Dongxue Li,[1] Guangang Tian,[1] Qing Li,[1] Yaoqi Zhou,[1] Suyuan Chen,[1] Hui-Zhen Nie,[1] Yujun Hao,[1] Jian Song,[4] Xue-Li Zhang,[1] Jan Sundquist,[5,6] Kristina Sundquist,[5,6] Jun Li,[1] Shu-Heng Jiang,[1] Zhi-Gang Zhang,[1] and Jianguang Ji[5]

[1]State Key Laboratory of Oncogenes and Related Genes, Shanghai Cancer Institute, Ren Ji Hospital, School of Medicine, Shanghai Jiao Tong University, Shanghai 200240, China; [2]Department of Epidemiology and Health Statistics, School of Public Health, Fujian Medical University, FuZhou 350108, China; [3]Department of Radiation Oncology, Institute of Oncology, Affiliated Hospital of Jiangsu University, Zhenjiang 212013, China; [4]Department of Radiation Oncology, Ren Ji Hospital, School of Medicine, Shanghai Jiao Tong University, Shanghai 200127, China; [5]Center for Primary Health Care Research, Department of Clinical Sciences, Lund University, Malmö 20502, Sweden; [6]Department of Family Medicine and Community Health, Department of Population Health Science and Policy, Icahn School of Medicine at Mount Sinai, New York, NY 10029, USA

Existing evidence indicates that gut fungal dysbiosis might play a key role in the pathogenesis of colorectal cancer (CRC). We sought to explore whether reversing the fungal dysbiosis by terbinafine, an approved antifungal drug, might inhibit the development of CRC. A population-based study from Sweden identified a total of 185 patients who received terbinafine after their CRC diagnosis and found that they had a decreased risk of death (hazard ratio = 0.50) and metastasis (hazard ratio = 0.44) compared with patients without terbinafine administration. In multiple mouse models of CRC, administration of terbinafine decreased the fungal load, the fungus-induced myeloid-derived suppressor cell (MDSC) expansion, and the tumor burden. Fecal microbiota transplantation from mice without terbinafine treatment reversed MDSC infiltration and partially restored tumor proliferation. Mechanistically, terbinafine directly impaired tumor cell proliferation by reducing the ratio of nicotinamide adenine dinucleotide phosphate ($NADP^+$) to reduced form of nicotinamide adenine dinucleotide phosphate (NADPH), suppressing the activity of glucose-6-phosphate dehydrogenase (G6PD), resulting in nucleotide synthesis disruption, deoxyribonucleotide (dNTP) starvation, and cell-cycle arrest. Collectively, terbinafine can inhibit CRC by reversing fungal dysbiosis, suppressing tumor cell proliferation, inhibiting fungus-induced MDSC infiltration, and restoring antitumor immune response.

INTRODUCTION

Colorectal cancer (CRC) is the third most commonly diagnosed malignancy and the second leading cause of cancer death.[1] Although the prognosis of CRC has continuously improved in recent decades,[2,3] there is a need to develop effective therapeutic strategies against CRC. Extensive studies indicate that the gut microbiota shapes the adaptive and innate immune systems,[4] which, in turn, regulate the pathogenesis of inflammatory bowel disease[5] and the development of CRC.[6] Previous studies have focused mainly on the roles of gut bacteria in CRC progression.[7,8] The gut mycobiome was recently reported to play a role in CRC development based on the evidence that CRC patients were associated with mycobiome dysbiosis and altered fungal composition.[9–11] It is thus reasonable that antifungal treatments may be a new therapeutic strategy against CRC. Terbinafine is commonly used for the treatment of superficial mycosis. *In silico* analyses integrating the human metabolic model with transcriptomic data indicate that terbinafine may have an antitumor effect.[12,13] Evidence from mouse models revealed that terbinafine can regulate tumor progression and tumor angiogenesis.[14,15] In this study, we accessed clinical data from several national Swedish registers and aimed to explore whether the post-diagnostic use of terbinafine may be associated with reduced mortality and reduced risk of metastasis in patients with CRC compared with patients without

Received 29 July 2021; accepted 23 June 2022;
https://doi.org/10.1016/j.ymthe.2022.06.015.

[7]These authors contributed equally

Correspondence: Jianguang Ji, Center for Primary Health Care Research, Department of Clinical Sciences, Lund University, Malmö 20502, Sweden
E-mail: Jianguang.ji@med.lu.se
Correspondence: Zhi-Gang Zhang, State Key Laboratory of Oncogenes and Related Genes, Shanghai Cancer Institute, Ren Ji Hospital, School of Medicine, Shanghai Jiao Tong University, Shanghai 200240, China.
E-mail: zzhang@shsci.org
Correspondence: Shu-Heng Jiang, State Key Laboratory of Oncogenes and Related Genes, Shanghai Cancer Institute, Ren Ji Hospital, School of Medicine, Shanghai Jiao Tong University, Shanghai 200240, China.
E-mail: shjiang@shsci.org
Correspondence: Jun Li, State Key Laboratory of Oncogenes and Related Genes, Shanghai Cancer Institute, Ren Ji Hospital, School of Medicine, Shanghai Jiao Tong University, Shanghai 200240, China.
E-mail: junli@shsci.org

Please cite this article in press as: Hu et al., Terbinafine prevents colorectal cancer growth by inducing dNTP starvation and reducing immune suppression, Molecular Therapy (2022), https://doi.org/10.1016/j.ymthe.2022.06.015

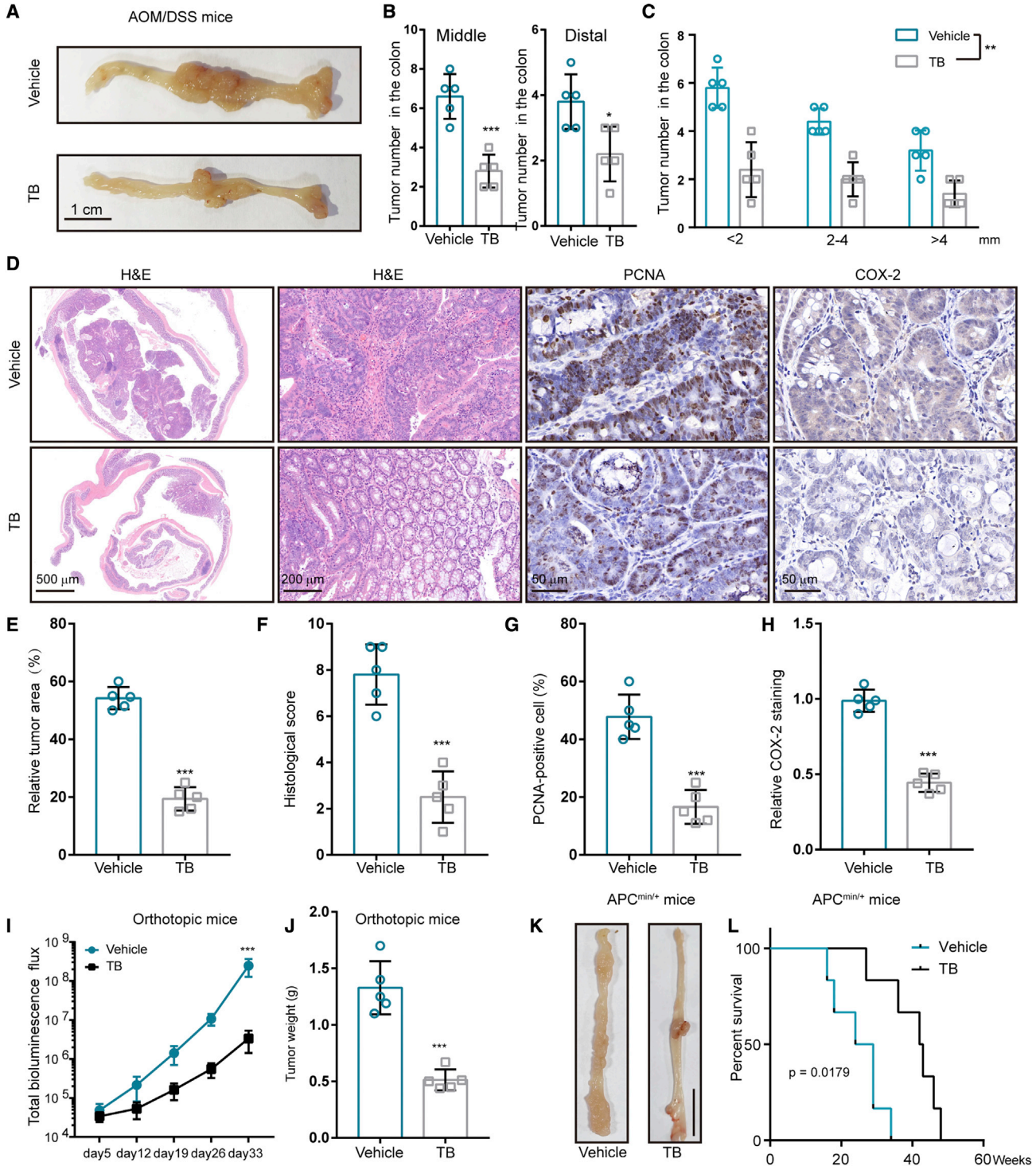

Figure 1. Terbinafine inhibits CRC development in mouse models

(A) Representative image of colons resected from AOM/DSS mice. The scale bar represents 1cm. (B and C) Statistical results of tumor numbers and sizes in terbinafine (TB)-treated mice and mice treated with vehicle (n = 5). (D) Histological analysis of colon tumors by hematoxylin and eosin (H&E) stain, PCNA, and COX-2 staining. (E and F) Statistical results of the tumor area and histological score in TB-treated mice and vehicle control mice (n = 5). (G and H) Percentages of PCNA- and COX-2-positive cells in colon tumors (n = 5). (I) Quantification of the total luminescence flux in mice bearing orthotopic CRC tumors, as measured by *in vivo* imaging system (IVIS) (n = 5). (J) Tumor weights

(legend continued on next page)

terbinafine use. We further evaluated the underlying mechanisms of the antitumor effect of terbinafine using multiple mouse models of CRC.

RESULTS

Post-diagnostic use of terbinafine is associated with a lower risk of death and metastasis in patients with CRC

A total of 185 patients, including 135 men and 50 women, received systemic treated with terbinafine after their diagnosis of CRC (Tables S1 and S2). Among them, the mean age at diagnosis of CRC was 65.7 years (n = 45 for age group <60 years; n = 34 for age group 60–64 years; n = 38 for age group 65–69 years; n = 68 for age group 70+ years). The mortality rate was 19.84 per 1,000 person-years (the summary of the number of patients in the group by multiplying the number of years that each patient being followed in the study) due to CRC, and it was 38.22 per 1,000 person-years among matched controls. After accounting for a range of demographic and clinical factors, the patients who received systemic terbinafine had a reduced risk of cause-specific death (hazard ratio [HR] = 0.50, 95% confidence interval [CI] = 0.28–0.88) compared with the controls. To explore the effect of the systemic use of terbinafine on metastasis, we excluded patients who had been diagnosed with metastatic cancer before the administration of terbinafine, and a total of 143 CRC patients were included in the analysis. Systemic use of terbinafine was associated with a lower risk of metastasis (HR = 0.44; 95% CI = 0.21–0.92). By lagging the exposure to terbinafine for 6 months (accounting for biological latency; Table S3), we found that the reduced risk of mortality and metastasis remained consistent with the main results ($HR_{mortality}$ = 0.51; $HR_{metastasis}$ = 0.41). In addition, the use of terbinafine before the diagnosis of CRC did not show an association with mortality and metastasis ($HR_{mortality}$ = 0.89, 95% CI = 0.71–1.11; $HR_{metastasis}$ = 0.88, 95% CI = 0.67–1.15), indicating that terbinafine use before the diagnosis of CRC may not affect CRC progression. Additionally, topical use of terbinafine was not associated with the risk of death and metastasis ($HR_{mortality}$ = 0.82, 95% CI = 0.61–1.10; $HR_{metastasis}$ = 0.94, 95% CI = 0.62–1.41), indicating that the antitumor effect of terbinafine should act on the pathogenic fungi in the gut. The risk of death or metastasis showed a dose-response relationship with the cumulative dose of terbinafine (Table S4).

Terbinafine treatment prevents CRC progression in multiple mouse models

To investigate the potential antitumor effects of terbinafine in CRC, the azoxymethane/dextran sodium sulfate (AOM/DSS)-induced CRC model,[16] orthotopic CRC mouse models,[17] and adenomatous polyposis coli ($APC^{min/+}$)[18] mouse models were applied. Among AOM/DSS-induced mice, the number of tumors in the distal and middle regions was 43% lower than that in the vehicle controls. The size of tumors was reduced 50% in the distal and middle regions of the colon compared with that in the vehicle controls (Figures 1A–1C and S1A). Hematoxylin and eosin staining revealed reduced epithelial hyperplasia and malignancy in terbinafine-treated mice (Figures 1D–1F). Immunohistochemistry (IHC) analysis revealed that the average percentage of proliferating cell nuclear antigen (PCNA)-positive cells in tumor tissues reduced from 70% to 32% upon terbinafine treatment. Additionally, the cyclooxygenase-2 (COX-2) intensity was 57% lower in tumor tissues derived from terbinafine-treated mice than that from vehicle controls (Figures 1D, 1G, and 1H). In the orthotopic mouse model of CRC, terbinafine treatment delayed orthotopic tumor growth (Figures 1I, S1B, and S1C), with a tumor burden from reduced 1.3 g to 0.6 g and a longer median survival time from 39 to 53 days compared with those of the vehicle controls (Figures 1J and S1D). Considering the important roles of APC mutation in human CRC, we established a CRC model with transgenic $APC^{min/+}$ mice (Figure S1E). Consistent with the results observed in the other two mouse models, terbinafine significantly inhibited tumor progression, with a longer median survival time from 22 to 43 weeks compared with that of the vehicle controls (Figures 1K, 1L, and S1F). These data indicate that terbinafine treatment prevents tumor progression in multiple mouse models of CRC.

Terbinafine treatment alters the fungal landscape and suppresses MDSC expansion

We next explored whether the antitumor effect of terbinafine was mediated by its fungicidal abilities. In mice with AOM/DSS-induced tumors, the total colonic fungal load in the feces shrank 67% after terbinafine treatment (Figure 2A). Compared with vehicle control mice, terbinafine-treated mice had decreased numbers of operational taxonomic units (OTUs) (Figure 2B). Principal component analysis (PCA) based on Bray-Curtis dissimilarity at the genus level revealed distinct fungal landscapes between the vehicle control and terbinafine-treated mice (Figure 2C). Internal transcribed spacer (ITS) sequencing revealed that Ascomycota and Basidiomycota, the dominant fungal phyla in mice with AOM/DSS-induced CRC, differed significantly between the vehicle and terbinafine-treated mice (Figure 2D). Further analysis showed that mice administered with terbinafine had a decreased abundance of *Candida*, *Mycosphaerella*, and *Articulospora* and an increased abundance of *Clavulinopsis* compared with the controls (Figures 2E and 2F). Given that fungi are heavily involved in MDSC expansion,[19] we further examined the alterations of MDSCs in the tumor tissue. Compared with the control mice, terbinafine-treated mice showed diminished proportions of MDSCs in the tumor tissue (Figures 2G and 2H). In addition, the antitumor immune cells, including the activated $CD8^+$ (Figures S2A–2C) and $CD4^+$ cells, were significantly increased in tumor tissues from terbinafine-treated mice compared with the vehicle controls (Figure H). Accordingly, flow cytometry analysis showed that terbinafine treatment also reduced the proportions of MDSCs in $APC^{min/+}$ mice

and relative proportions of apoptotic cells in orthotopic xenografts (n = 5). (K) Representative image of colons resected from $APC^{min/+}$ mice. The tumor multiplicities were 4.6 ± 1.1 (vehicle) and 2.7 ± 1.3 (TB), and the tumor incidence was 100% in $APC^{min/+}$ mice. The scale bar represents 1cm. (L) Overall survival of $APC^{min/+}$ mice with or without TB treatment (n = 10). Data are presented as mean ± SD. (B, E–G, J) Unpaired two-tailed Student's t test. (C and I) One-way ANOVA with Bonferroni correction. (L) Log rank test; $^{**}p < 0.01$ and $^{***}p < 0.001$.

Please cite this article in press as: Hu et al., Terbinafine prevents colorectal cancer growth by inducing dNTP starvation and reducing immune suppression, Molecular Therapy (2022), https://doi.org/10.1016/j.ymthe.2022.06.015

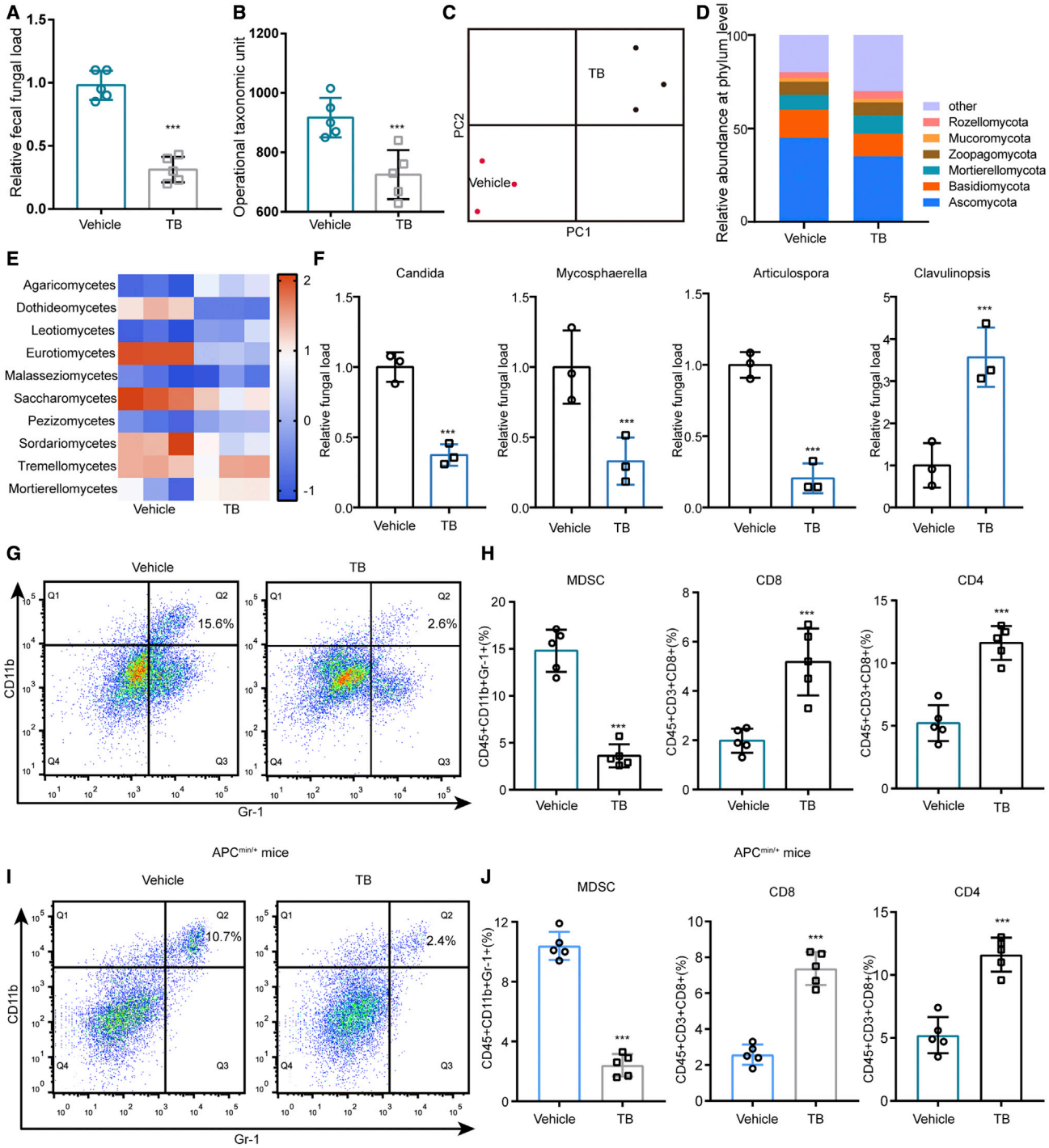

Figure 2. TB alters the fungal landscape and MDSC expansion

(A) Fecal fungal load in vehicle- and TB-treated AOM/DSS mice (n = 5). Mouse fecal DNA was extracted from stools and quantified by 18S rRNA. (B) Operational taxonomic units (OTUs) in feces, as determined by internal transcribed spacer (ITS) sequencing (n = 3). (C) Principal component analysis based on fungal ITS sequencing of fecal samples from AOM/DSS mice (n = 3). (D) Fungal analysis at the phylum level in the feces of AOM-DSS mice treated with TB or vehicle. (E) Heatmap of the fungal load at the class level in the feces of AOM-DSS mice treated with TB or vehicle. (F) Representative fungal alterations at the species level. (G and H) Proportion of MDSCs, $CD8^+$ cells, and $CD4^+$ cells in tumor tissues resected from AOM-DSS mice (n = 5). (I and J) Proportion of MDSCs, $CD8^+$ cells, and $CD4^+$ cells in tumor tissues resected from $APC^{min/+}$ mice (n = 5). Data are presented as mean ± SD. (A, B, F, H, J) Unpaired two-tailed Student's t test. ***p < 0 .001.

Please cite this article in press as: Hu et al., Terbinafine prevents colorectal cancer growth by inducing dNTP starvation and reducing immune suppression, Molecular Therapy (2022), https://doi.org/10.1016/j.ymthe.2022.06.015

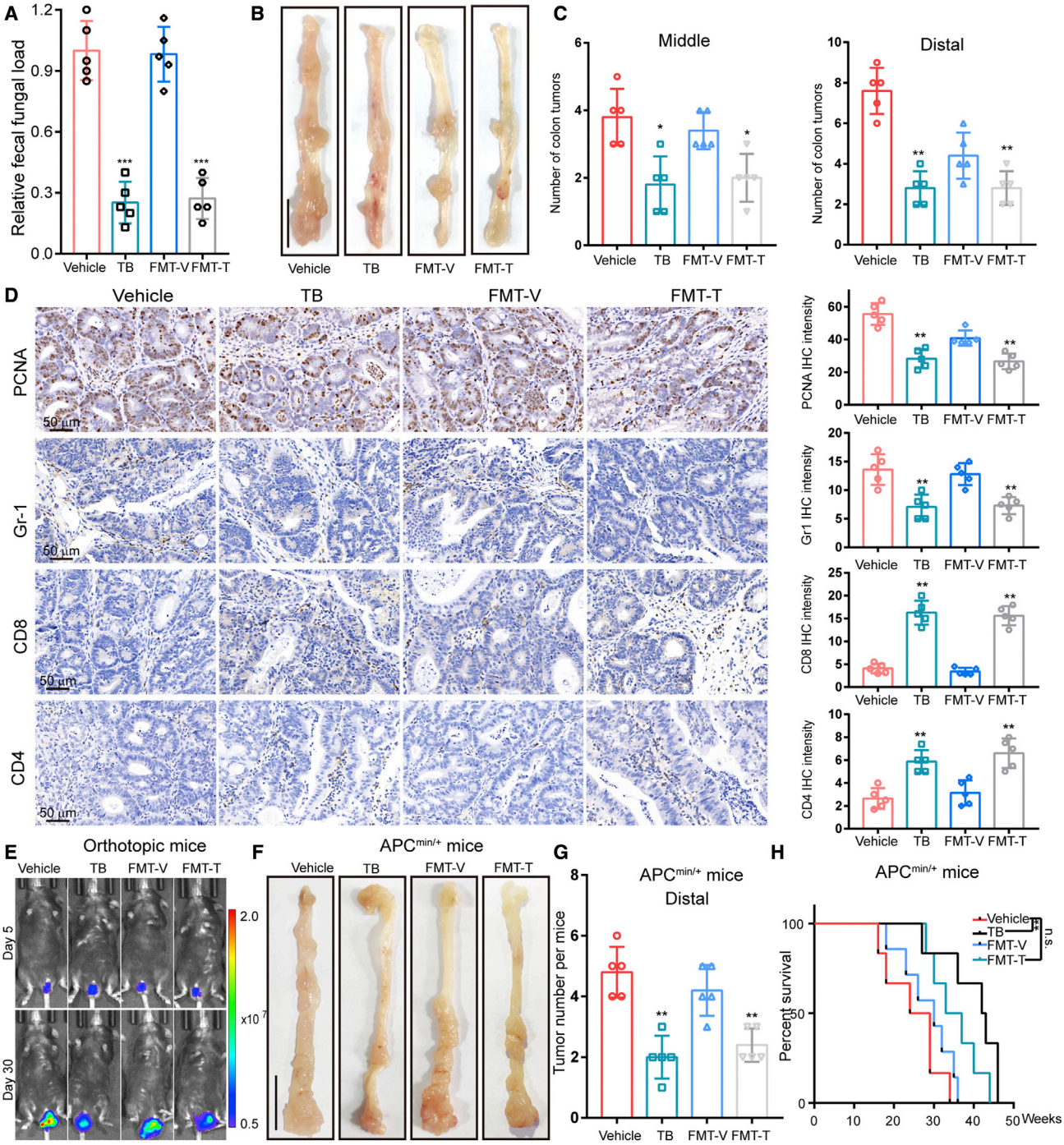

Figure 3. Effects of FMT on TB-treated mice

(A and B) Fecal fungal load of AOM/DSS mice treated with vehicle, TB, TB plus FMT- (fecal microbiota from the vehicle group mice [FMT-V]), and TB plus FMT (fecal microbiota from the TB group mice [FMT-T]) (n = 5). Mouse fecal DNA was extracted from stools and quantified by 18S rRNA. (B) Representative image of colons resected from AOM/DSS mice. The scale bar represents 1cm. (C) Statistical results of tumor numbers and sizes in AOM/DSS mice, tumor number in the middle colon (left), tumor number in the distal colon (right) (n = 5). (D) IHC staining of PCNA, Gr-1, CD8, and CD4 in tumors resected from AOM/DSS mice (left). Statistical results of IHC intensity (right). (E) Representative bioluminescence image of mice orthotopically implanted with luciferase-expressing MC38 cells administered vehicle, TB, TB plus FMT-V, or TB plus FMT-T.

(legend continued on next page)

(Figures 2I and 2J) and mice with orthotopic implantation (Figure S2D). Collectively, these data indicate that terbinafine administration could evoke an antitumor immune response by inhibiting fungus-induced MDSC expansion.

Fungal restoration partially reverses the antitumor effect of terbinafine on CRC

Next, fecal microbiota transplantation (FMT) was employed to further reveal the antitumor mechanisms of terbinafine. Transplantation of fecal microbiota obtained from mice in the vehicle group (FMT-V) almost completely restored the fungal load (Figures 3A and S3A) and partially restored the tumor burden in AOM/DSS-induced mice (Figures 3B and 3C). Transplantation of fecal microbiota from terbinafine-treated mice (FMT-T) did not affect the tumor burden. The proportion of MDSCs in mice that received FMT-V was restored to a level similar to that in mice in the vehicle group (Figure S3B). IHC staining showed a marked decline of MDSCs and an increase of $CD4^+$ and $CD8^+$ T cells following terbinafine treatment (Figure 3D). Furthermore, FMT-V enhanced MDSC expansion, and reduced $CD8^+$ and $CD4^+$ staining intensities to levels similar to the controls. However, PCNA staining showed that FMT-V did not reverse cancer cell proliferation to the control level (Figure 3D). Consistent with this finding, restoration of the colonic fungal load by FMT-V only partially reversed the inhibitory effects of terbinafine on orthotopic tumors (Figures 3E, S3C, and S3D) and $APC^{min/+}$ mice (Figures 3F–3H and S3E). These data indicate that the antitumor effect of terbinafine in CRC may not be fully dependent on its fungicidal abilities.

Terbinafine directly suppresses CRC cell growth by interrupting nucleotide biosynthesis

CRC cells were treated with different concentrations of terbinafine (1–50 μM) (Figure S4A). after the treatment, the viability of HCT116, HT29, LoVo, and DLD1 cells was significantly reduced (Figure 4A). The colony formation assay indicated that terbinafine suppressed CRC cell proliferation (Figures 4B and S4B). Terbinafine markedly reduced the tumor burden of CRC cell-derived tumor xenografts (Figure 4C). Gene set enrichment analysis (GSEA) was performed to analyze the difference in global gene expression between terbinafine-treated cells and the vehicle control cells. The differentially expressed genes were enriched in the cell cycle, DNA replication, pyrimidine metabolism, and purine metabolism pathways (Figure 4D). Flow cytometry indicated that CRC cells treated with terbinafine exhibited a decrease in the proportion of cells in the S phase and a concomitant increase in the proportion of cells in the G1 phase (Figures S4C and S4D). We assessed the nucleotide synthesis rate in these cells under terbinafine treatment using ^{13}C-labeled glucose tracing. We observed a greater reduction in the concentration of newly synthesized dNTPs and R5P compared with vehicle control cells (Figure 4E). Exogenous dNTP supplementation by the hypotonic shift method[20] largely reversed the growth inhibition caused by terbinafine (Figure 4F). These results indicate that terbinafine has a direct cytotoxic effect on CRC cells by interrupting *de novo* nucleotide biosynthesis.

Terbinafine disrupts the pentose phosphate pathway by targeting squalene epoxidase

The target of terbinafine is squalene epoxidase (SQLE), which was reported to be involved in nonalcoholic fatty liver disease-induced hepatocellular carcinoma (HCC) by regulating DNA methyltransferase 3A expression and the Akt-mammalian target of rapamycin (mTOR) pathway.[15] We silenced SQLE in HCT116, HT29, LoVo, and DLD1 cells by short hairpin RNA (shRNA) (Figures S5A and S5B). SQLE knockdown significantly reduced CRC cell viability (Figure S5C), and their viability was not affected by terbinafine after SQLE silencing (Figure 5A). Overexpression of SQLE promoted CRC cell proliferation, which was abolished by terbinafine treatment (Figures S5D–S5F). In addition, SQLE expression was upregulated in CRC tissues compared with adjacent tissues (Figure S5G). The growth of CRC-patient-derived xenografts with a high SQLE expression was significantly inhibited upon terbinafine treatment (Figures 5B and S6A). SQLE is known as the second rate-limiting enzyme in intracellular cholesterol biosynthesis and could inhibit the production of $NADP^+$ from NADPH. However, exogenous cholesterol supplementation did not reverse the inhibition of nucleotide synthesis by terbinafine (Figure S6B). We found that the ratio of $NADP^+$ to NADPH in CRC cells was decreased upon terbinafine treatment, resulting in cell apoptosis (Figures 5C and S6C). As the ratio of $NADP^+$ to NADPH is the main modulator of glucose-6-phosphate dehydrogenase (G6PD) in the pentose phosphate pathway (PPP),[21] we performed an enzymatic activity assay and found that the activity of G6PD decreased dramatically in human and mouse CRC cells after treatment with terbinafine (Figure 5D). Inhibiting G6PD by 6-AN[22] and DHEA,[23] as well as shRNA, abolished the enhancement of dNTP and R5P synthesis due to overexpression of SQLE (Figures 5E and 5F). The growth advantages due to SQLE overexpression were reversed by the G6PD inhibitors of 6-AN and DHEA (Figure 5G) in cancer cells and by genetic inhibition of G6PD with shRNA in a mouse model (Figure 5H). These results indicate that terbinafine treatment suppresses G6PD activity through an SQLE-mediated reduction in the ratio of $NADP^+$ to NADPH, resulting in disruption of the PPP and nucleotide biosynthesis, eventually leading to cell-cycle arrest and cell growth inhibition.

Terbinafine suppresses CRC development by inhibiting the expansion of MDSCs and by inducing cytotoxic effects on CRC cells

$APC^{min/+}$ mice were administered with an anti-Ly6G antibody alone to deplete MDSCs or in combination with terbinafine (Figure S7A).

(F) Representative image of colons resected from $APC^{min/+}$ mice treated with vehicle, TB, TB plus FMT-V, and TB plus FMT-T. The scale bar represents 1 cm. (G) Tumor number statistical results of $APC^{min/+}$ mice in the distal colon. The tumor multiplicities were 9.3 ± 1.4 (vehicle), 4.9 ± 1.6 (TB), 7.6 ± 1.7 (TB plus FMT-V), and 4.3 ± 0.9 (TB plus FMT-T), and the tumor incidence was 100%. (H) Overall survival of $APC^{min/+}$ cells treated with vehicle, TB, TB plus FMT-V, and TB plus FMT-T. Data are presented as mean ± SD. (A, C, D, G) Unpaired two-tailed Student's t test. (H) Log rank test. *$p < 0.05$, **$p < 0.01$, and ***$p < 0.001$.

Please cite this article in press as: Hu et al., Terbinafine prevents colorectal cancer growth by inducing dNTP starvation and reducing immune suppression, Molecular Therapy (2022), https://doi.org/10.1016/j.ymthe.2022.06.015

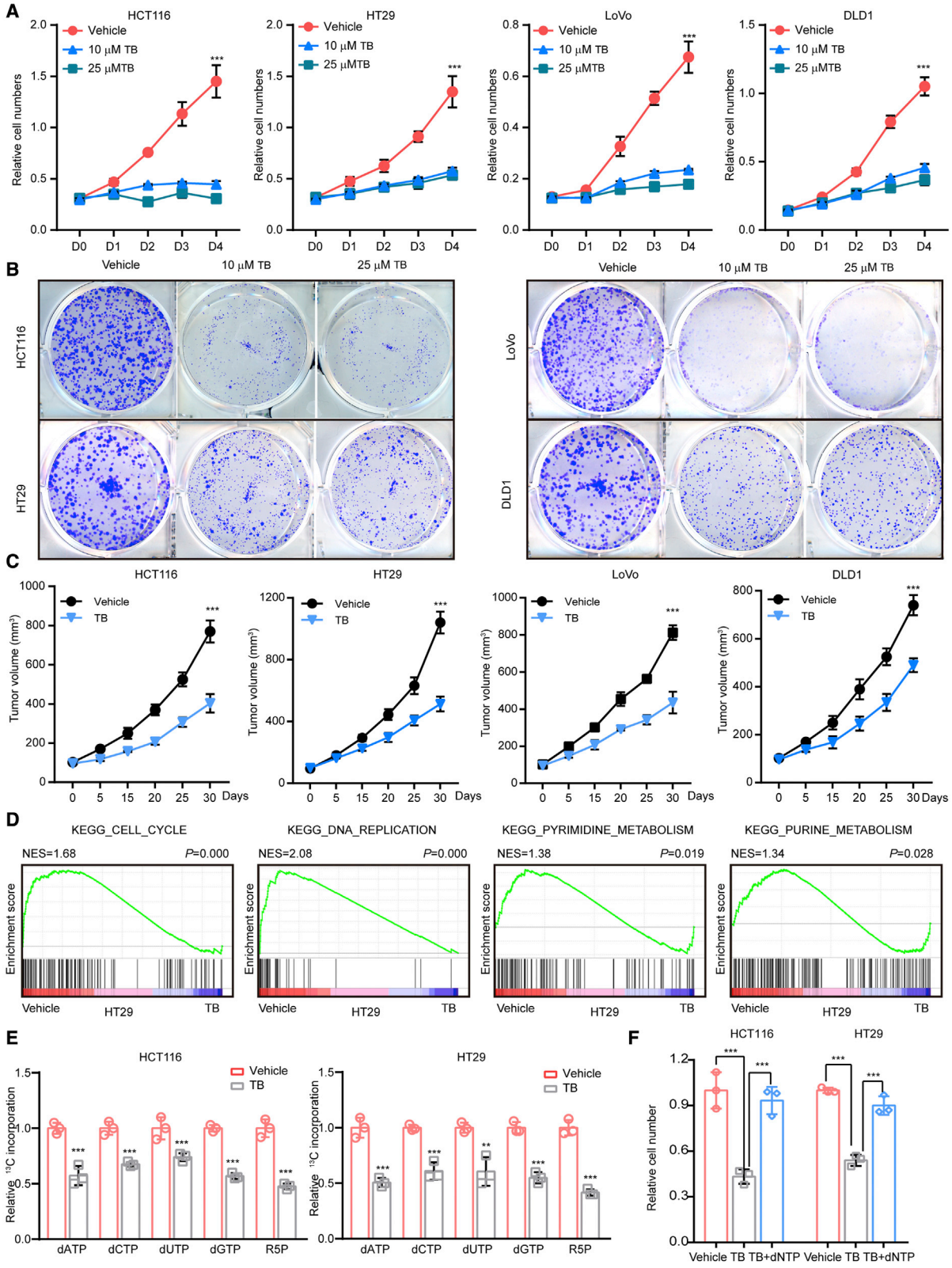

(legend on next page)

Please cite this article in press as: Hu et al., Terbinafine prevents colorectal cancer growth by inducing dNTP starvation and reducing immune suppression, Molecular Therapy (2022), https://doi.org/10.1016/j.ymthe.2022.06.015

As expected, anti-Ly6G therapy significantly decreased the proportion of MDSCs and ameliorated the progression of CRC (Figures 6A–6C). Combined treatment with the anti-Ly6G antibody and terbinafine provided additional benefits by reducing the tumor number and prolonging the overall survival time (Figures 6A–6D and S7B). IHC analysis showed that tumor tissues derived from mice treated with both terbinafine and anti-Ly6G antibody exhibited much lower levels of PCNA and Gr-1 staining than those from mice treated with the anti-Ly6G antibody alone (Figures 6E–6G). Furthermore, terbinafine treatment greatly reduced the ratio of NADP+ to NADPH and G6PD activity, while anti-Ly6G antibody alone did not show such an effect (Figures 6H and 6I). In the AOM/DSS-induced CRC model, we observed similar results (Figures S8 and S9). Bioluminescence imaging revealed that mice injected with shSQLE-expressing MC38 cells had smaller tumors and a longer survival time than control mice (Figures 6J–6L). Additionally, terbinafine treatment further delayed the progression of CRC in mice bearing orthotopic tumors formed by shSQLE-expressing MC38 cells (Figure 6M). Tumor tissues from terbinafine-treated mice or shSQLE-expressing MC38 cell-injected mice showed lower levels of G6PD activity (Figure 6N). Flow cytometry analysis revealed that terbinafine treatment but not SQLE silencing dramatically inhibited MDSC expansion (Figure 6O). These data indicate that terbinafine prevents CRC progression through two mechanisms: inhibiting fungus-induced MDSC expansion and exerting direct cytotoxic effects on CRC cells (Figure 7).

DISCUSSION

In this study, we combined comprehensive evidence from a population-based cohort study and multiple mouse models to evaluate the antitumor effects of terbinafine, a broad-spectrum fungicidal drug, on the development of CRC. The population-based study in Sweden showed that post-diagnostic use of terbinafine was associated with a lower risk of death and metastases compared with patients without using terbinafine. Terbinafine administration dramatically altered the gut fungal landscape, reduced MDSC infiltration, and recovered antitumor immune cells. In addition, terbinafine can directly inhibit CRC cell proliferation by targeting SQLE, thus reducing the ratio of $NADP^+$ to NADPH, suppressing the activity of G6PD, and resulting in nucleotide synthesis disruption and cell-cycle arrest. Our data indicate that terbinafine can be repurposed as an adjuvant for the treatment of CRC if further randomized clinical trials can confirm our findings.

To date, extensive evidence has revealed that microbes are crucial regulators of tumor development.[24,25] However, research on the fungal microbiome is relatively new, and our understanding of the fungal microbiome lags behind that of the bacterial microbiome. Recently, fungi have attracted attention after several studies have suggested that they are heavily involved in tumorigenesis. Wang et al. reported that gut fungal dysbiosis contributed to the development of colitis-associated cancer in a mouse model of CRC.[19] Aykut et al. observed an increased abundance and distinct composition of fungi in pancreatic cancer tissues from both humans and mice, which further activated the complement cascade, with cleavage of C3 into C3a and C3b, and promoted pancreatic cancer progression.[26] These studies indicated that antifungal treatment could be a therapeutic strategy for various cancers.

MDSCs, characterized as Gr-1+ and CD11b+ cells, have been reported to regulate immune responses,[27] leading to cancer invasion, and metastasis.[28] The dectin receptor on MDSCs could recognize the fungi and activate the downstream Syk-Card9 signaling axis, leading to intratumoral accumulation of MDSCs and suppression of the immune response.[29] A previous study reported that the accumulation of commensal fungi in the CRC tumor microenvironment could induce MDSC expansion,[11,19] which could be inhibited by administration of amphotericin B and fluconazole. Notably, the antifungal mechanisms of terbinafine differ from those of amphotericin B and fluconazole. Terbinafine selectively inhibits fungal squalene epoxidase, resulting in the suppression of ergosterol synthesis and toxic accumulation of squalene,[30] whereas amphotericin B binds to sterols in the fungal plasma membrane.[31] Fluconazole inhibits lanosterol-14-a-demethylase, an enzyme downstream squalene epoxidase that controls ergosterol synthesis.[32] Among these three antifungal drugs, terbinafine is the most recently US Food and Drug Administration (FDA)-approved drug and has the highest antifungal efficiency.[33,34]

In addition to its fungicidal ability, terbinafine directly suppressed the proliferation of CRC cells by targeting SQLE. Our results showed that SQLE expression is upregulated in CRC cells. Similarly, SQLE is overexpressed in nonalcoholic fatty liver disease-induced HCC,[15] and SQLE expression is associated with a poor prognosis in breast cancer.[35] As a rate-limiting enzyme in cholesterol synthesis, SQLE plays a crucial role in intracellular cholesterol hemostasis.[36] SQLE inhibition in HCC and prostate cancer inhibited cholesterol metabolism and suppressed cancer cell growth.[37] However, recent studies showed that the inhibition of the small cell lung cancer cells was due to the toxic accumulation of the SQLE substrate instead of the inhibition of the cholesterol biosynthesis pathway.[38,39] Consistent with this finding, our transcriptome analysis revealed cell-cycle arrest and nucleotide biosynthesis disruption in CRC cells upon terbinafine

Figure 4. Direct anti-tumor effect of TB on CRC cells

(A and B) Relative cell numbers and results of colony formation assays of HCT116, HT29, LoVo, and DLD1 cells treated with DMSO (vehicle), 10 μM TB, or 25 μM TB. (C) Growth curve of subcutaneous tumors in mice treated with TB (50 mg/kg) or DMSO (vehicle). (D) Gene set enrichment analysis (GSEA) using Kyoto Encyclopedia of Genes and Genomes (KEGG) gene sets to compare HT29 cells with HT29 cells treated with TB (25 μM) for 48 h. NES, normalized enrichment score. (E) Histograms of relative ^{13}C-labeled R-5-P and dNTP incorporation in vehicle- or TB-treated HCT116 and HT29 cells (n = 3). (F) Relative numbers of HCT116 and HT29 cells treated with DMSO (vehicle), 25 μM TB, or 25 μM TB plus dNTPs. Data are presented as mean ± SD. (A, C) One-way ANOVA with Bonferroni correction. (E and F) Unpaired two-tailed Student's t test. $^{**}p < 0.01$ and $^{***}p < 0.001$.

Please cite this article in press as: Hu et al., Terbinafine prevents colorectal cancer growth by inducing dNTP starvation and reducing immune suppression, Molecular Therapy (2022), https://doi.org/10.1016/j.ymthe.2022.06.015

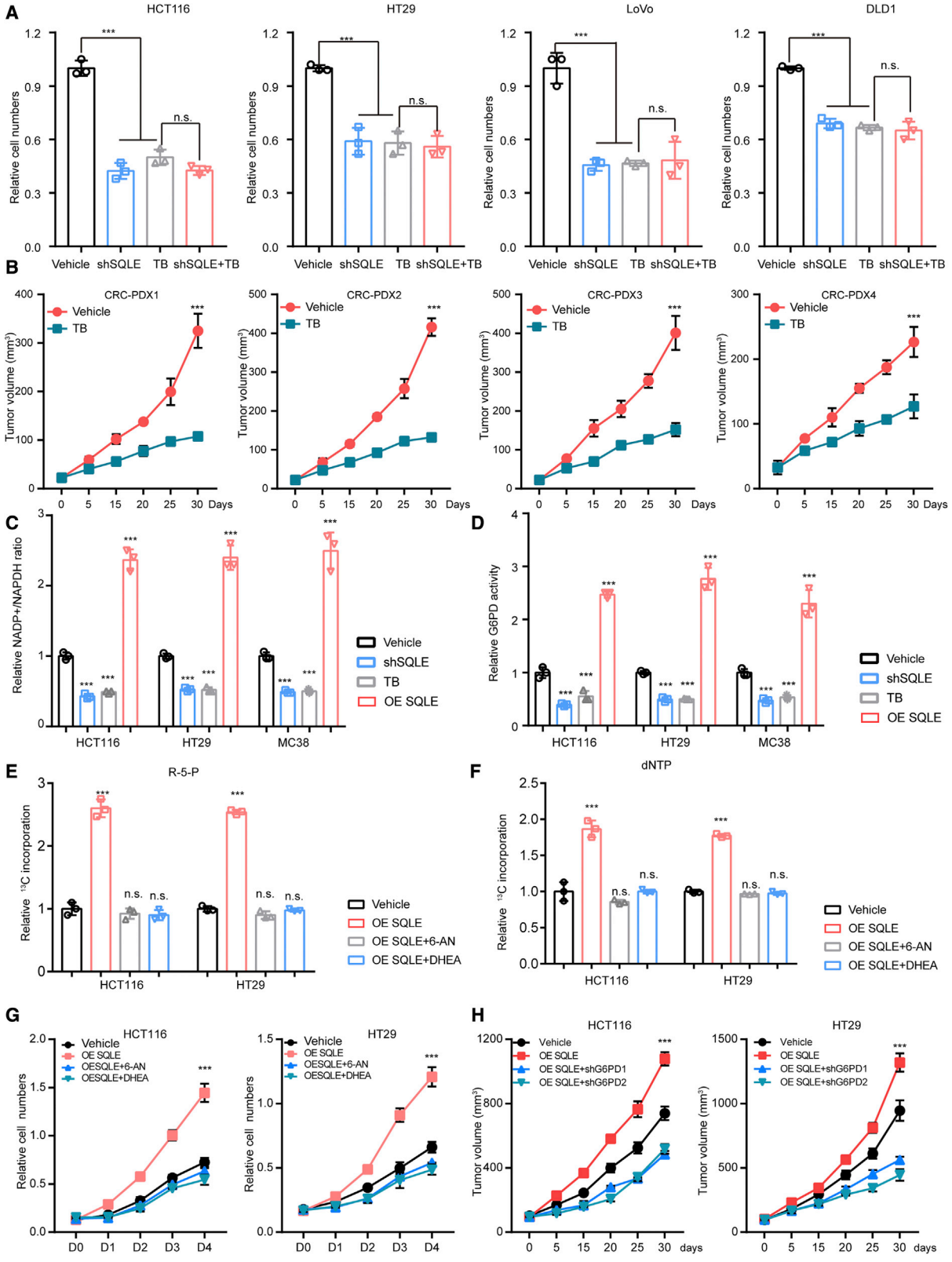

(legend on next page)

treatment. Exogenous cholesterol supplementation did not reverse the inhibition of nucleotide synthesis induced by SQLE inhibition. Our study showed that SQLE inhibition greatly decreased the $NADP^+$/NADPH ratio and modulated the enzymatic activity of G6PD, resulting in disruption of R5P and dNTP synthesis. The results of genetic and pharmacological inhibition of G6PD further confirmed its intermediary role in terbinafine-induced inhibition of cell growth.

Although terbinafine is widely used clinically, more research is required to determine the feasibility of treating CRC patients with terbinafine alone or in combination with standard first-line CRC therapeutic strategies. Furthermore, because CRC is a highly heterogeneous disease,[40] evaluations should be performed to determine whether terbinafine treatment is suitable for all the patients with CRC.

This study reveals the antitumor effect of terbinafine based on the population-based study and multiple mouse models of CRC. The underlying mechanisms of terbinafine against CRC were due to its ability to inhibit fungus-induced MDSC expansion and exert direct cytotoxic effects on CRC cells, both of which evoke antitumor immune responses and suppress cancer cell growth.

MATERIALS AND METHODS

Ethics statement

The population-based cohort study was approved by the Ethics Committee at Lund University. The Ethics Approval ID is Dnr 2012/795. The ethical approval of the CRC specimen was obtained from the Research Ethics Committee of Ren Ji Hospital, School of Medicine, Shanghai Jiao Tong University. The Ethics Approval ID is RJ2018-064. Animal experiments were performed following the recommendations in the Guide for the Care and Use of Laboratory Animals and relevant Chinese laws and regulations. The protocol was approved by the Institutional Animal Care and Use Committee (IACUC) of Shanghai Jiao Tong University, and the Animal Protocol number is A20201204.

National population-based cohort study in Sweden

All patients who were diagnosed with CRC between July 2005 and December 2014 were identified from the Swedish Cancer Registry by using the 10th International Classification of Disease (International Classification of Diseases [ICD]-10 codes C18, C19, and C20).[41] These patients with CRC were further linked to the Swedish Prescribed Drug Register to determine information about their subsequent use of terbinafine.[42] The Anatomical Therapeutic Chemical (ATC) classification system was used to classify all prescribed drugs. Using the ATC code D01BA02, we identified individuals who had used terbinafine orally (systemic use). Furthermore, we identified individuals who had used terbinafine topically (topical use) by using ATC code D01AE15.[43] Cumulative doses of the systemic use of terbinafine were calculated as the sum of the defined daily dose (DDD) for all prescriptions during the follow-up period. To improve the comparability, five CRC patients who did not use terbinafine were randomly selected for each patient with systemic use of terbinafine using nearest-neighbor propensity score matching. Patients with CRC were further linked with the Total Population Register and with the Population Housing Census to obtain information on individual-level characteristics and with the Cause of Death Register to identify the date of death as well as the cause of death. From the Cause of Death Register, we identified all patients with CRC who had died between July 2005 and December 2015. The primary outcome was death due to CRC as the primary cause of death (ICD-10 codes C18–C20). The secondary outcome was metastatic cancer (ICD-10 codes C77, C78, and C79). From the National Patient Register (NPR), we identified all patients with CRC who had been diagnosed with metastatic cancer.

To account for immortal time bias, we used time-dependent Cox regression to calculate HRs and 95% CIs for CRC mortality and metastasis associated with the post-diagnostic use of terbinafine, which meant that terbinafine use was included as a time-dependent variable in the regression model. Patients may have moved from a follow-up period of non-exposure (from diagnosis of CRC to the administration of terbinafine) to a period of exposure (from the use of terbinafine and thereafter of the follow-up). Several demographic and clinical factors were included in the multivariate model to account for their potential residual confounding effects, including sex, country of birth (Sweden, European countries, and others), highest educational level (1–9, 10–11, and 12+), individual disposable income (lowest, middle-low, middle-high, and highest), comorbidities (diabetes, hypertension, chronic ischemic heart disease, and chronic obstructive pulmonary disease), the region at diagnosis (big cities and southern and northern Sweden), age at diagnosis of CRC, year at diagnosis of CRC, and stage of CRC (stages 1, 2, 3, and 4). We censored individuals (i.e., treated them as no longer under observation or at risk of the study outcome) at the time of death from CRC, at the end of the follow-up period (December 31, 2015) or at the time of emigration, whichever came first. The proportional hazards assumption was tested using cumulative martingale residuals.

Figure 5. TB inhibits the pentose phosphate pathway by targeting SQLE

(A) Relative numbers of HCT116, HT29, LoVo, and DLD1 cells treated with DMSO + sh scramble (referred to as vehicle), shSQLE, 25 μM TB, or shSQLE plus 25 μM TB. shSQLE and TB are compared with vehicle. TB is compared with shSQLE + TB. (B) The response of patient-derived xenografts (PDX) with high SQLE expression to TB (n = 5). CRC PDXs are CRC-patient-derived xenografts. (C) $NADP^+$/NADPH ratio in human and mouse CRC cells treated with vehicle control, shSQLE, 25 μM TB, or OE SQLE. OE, overexpression. (D) G6PD activity in human and mouse CRC cells treated with vehicle control, shSQLE, 25 μM TB, or OE SQLE. (E and F) Histograms of relative ^{13}C-labeled R-5-P and dNTP incorporation in HCT116 and HT29 cells treated with vehicle control, OE SQLE, OE SQLE plus 6-AN, or OE SQLE plus DHEA (n = 3). (G) Relative numbers of HCT116 and HT29 cells treated with vehicle control, OE SQLE, OE SQLE plus 6-AN, or OE SQLE plus DHEA. (H) Growth curve of subcutaneous tumors in mice implanted with vehicle control, OE SQLE, OE SQLE plus shG6PD 1, and OE SQLE plus shG6PD 2 cells (n = 5). Data are presented as mean ± SD. (A, C–F) Unpaired two-tailed Student's t test. (B, G, H) One-way ANOVA with Bonferroni correction; n.s., not significant; $p > 0.05$; ***$p < 0.001$.

Please cite this article in press as: Hu et al., Terbinafine prevents colorectal cancer growth by inducing dNTP starvation and reducing immune suppression, Molecular Therapy (2022), https://doi.org/10.1016/j.ymthe.2022.06.015

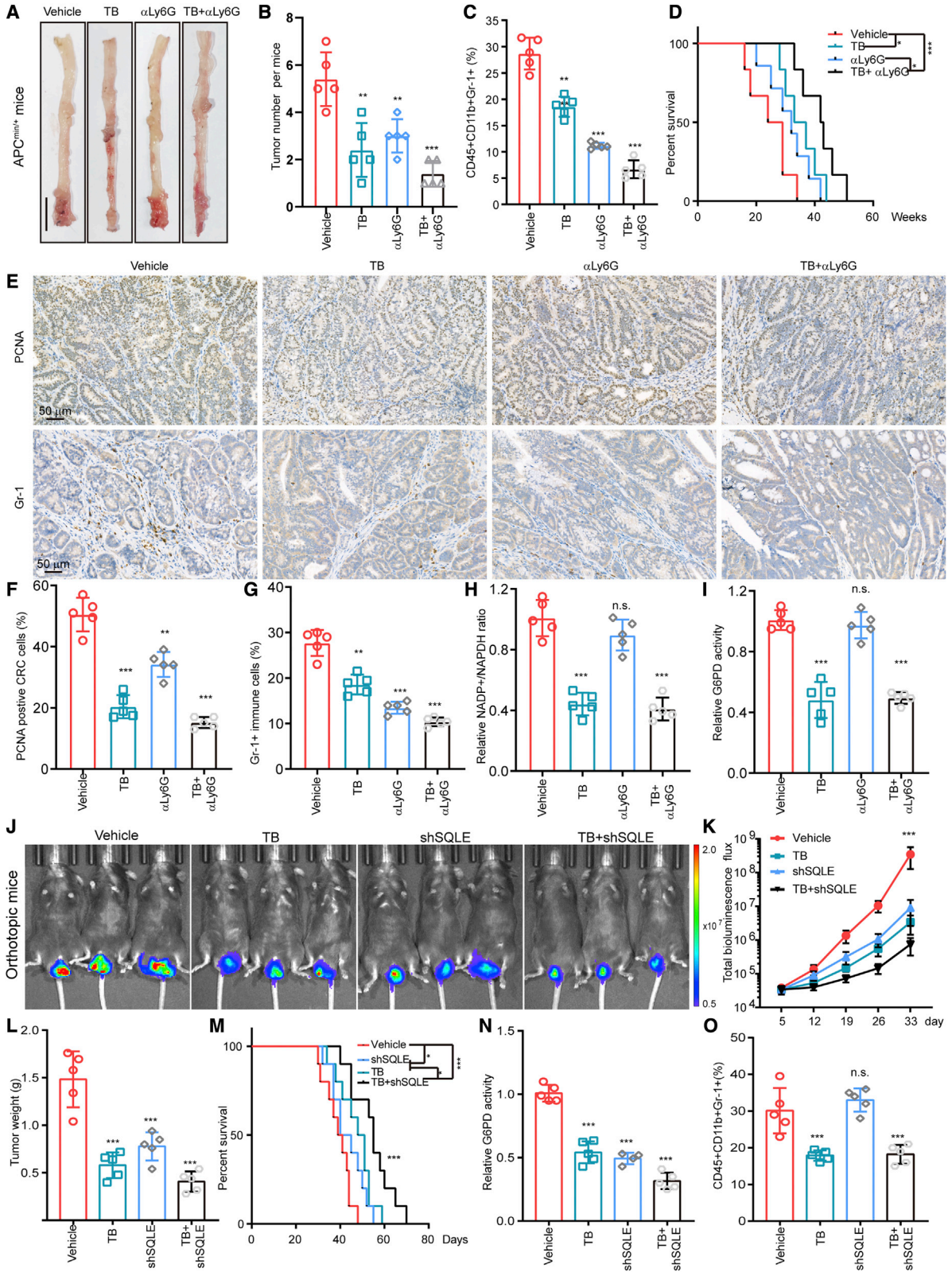

(legend on next page)

All analyses were performed using SAS version 9.2 (SAS Institute, Cary, NC, USA).

Animal models

AOM/DSS model

The AOM/DSS model was established according to the standard method.[16] Briefly, 5- to 6-week-old C57BL/6 male mice (n = 5) were intraperitoneally injected with AOM (10 mg/kg) on day 1. After 5 days, 2.5% DSS was added to the drinking water for seven consecutive days. Three cycles of DSS treatment were used. Mice were administered with terbinafine (20 mg/kg) by intraperitoneal injection during the first cycle of DSS. For MDSC depletion, an anti-Ly6G antibody (25 μg) was injected intraperitoneally every 3 days after AOM injection. The experiments were repeated three times.

$Apc^{min/+}$ model

C57BL/6J-$Apc^{min/+}$ mice were kind gifts from Professor Dali Li at the East China Normal University. Male $APC^{min/+}$ mice (n = 5 in each group) at 6 weeks old were exposed to the same dose of terbinafine and anti-Ly6G antibody treatments as the AOM/DSS mouse model. Polyp counts were performed when mice reached 20 weeks of age. The experiments were repeated three times.

Orthotopic mouse model

The orthotopic CRC mouse model was constructed by injecting luciferase-expressing MC38 cancer cells using the lumen implantation technique. Before the surgery, mice were randomly divided into three groups treated with DMSO plus PBS (vehicle), terbinafine (50 mg/kg), or terbinafine (50 mg/kg) plus FMT for 2 weeks (n = 5 in each group). For the FMT experiments, fresh feces collected from wild-type (WT) C57BL/6N mice were suspended and orally given to terbinafine-treated mice. The mice were anesthetized by isoflurane inhalation in a supine position. A blunt-ended hemostat was inserted into the anus of the mouse, and the hemostat was angled toward the mucosa and opened slightly such that a single mucosal fold could be clasped by closing the hemostat to the first notch. Next, 5×10^5 luciferase-expressing MC38 cells suspended in 10 μL of PBS were transplanted into the mucosa, followed by bioluminescence imaging every 7 days. The experiments were repeated three times. Total flux emission was quantified using Living Image software, version 4.5.3.

Subcutaneous and CRC-patient-derived xenograft model

Athymic male nu/nu mice aged from 6 to 8 weeks were used for the subcutaneous and CRC-patient-derived xenograft model. Subcutaneous implant models were established by subcutaneous injection at a total cell number of 1×10^6 in the right-back flank of mice. For the CRC-patient-derived xenograft model, surgical specimens from colorectal cancer patients were physically separated into small pieces (2–3 mm) and subcutaneously transplanted into nude mice. Once tumors were grown, xenografts were resected. Tumor diameters were monitored with digital caliper every 5 days. Mice were sacrificed after 30 days and the tumor was isolated and weighed. Tumor volumes were calculated by volume = $0.5 \times \text{length} \times \text{width}^2$.

All colon tissues, tumor tissues, feces, spleens, and peripheral blood were collected after the mice were euthanized.

Cell culture

The human CRC cell lines HCT116, HT29, LoVo, DLD1, human normal intestinal epithelial cell line NCM460, and mouse CRC cell line MC38 were preserved at Shanghai Cancer Institute, Renji Hospital, School of Medicine, Shanghai Jiao Tong University. Cells were grown in the suggested culture medium supplemented with 10% fetal bovine serum (FBS; Gibco), 100 U/mL penicillin, and 100 μg/mL streptomycin at 37°C with 5% CO_2. The base medium for HCT116, HT29, LoVo, and DLD1 cells was McCoy's 5A, and Dulbecco's modified Eagle's medium (DMEM) was used for NCM460 and MC38 cells. All cell lines underwent verification in January 2019 by Shanghai Cancer Institute and regular testing (every 4 months) to ensure no contamination with mycoplasma.

Cell viability assay

Cell viability was determined by using Cell Counting Kit-8 (SB-CCK8S, ShareBio, China) according to the manufacturer's instructions. Briefly, cells with the indicated treatment were seeded in a 96-well plate at the density of 3,000 cells/well, which was performed in quintuplicate. At the indicated time points, CCK-8 was added to the well and incubated for 1 h at 37°C. Absorbance at 450 nm was measured by a microplate reader (M1000 PRO, TECAN). The experiments were performed in quintuplicate and conducted three times.

Figure 6. The antitumor effect of TB is dependent on the inhibition of MDSC expansion and direct cytotoxicity to CRC cells

(A) Representative image of colons resected from vehicle-, TB-, anti-Ly6G- (referred to as αLy6G), and TB plus anti-Ly6G antibody-treated $APC^{min/+}$ mice (n = 5). (B) Tumor numbers in the colon of $APC^{min/+}$ mice treated with DMSO (vehicle), TB, anti-Ly6G, or TB plus anti-Ly6G (n = 5). The tumor multiplicity was 5.3 ± 1.8 (vehicle), 1.9 ± 1.5 (TB), 3.6 ± 2.1 (anti-Ly6G), and 1.3 ± 0.7 (TB plus anti-Ly6G), and the tumor incidence was 100%. (C) Proportions of MDSCs in colon tumors of $APC^{min/+}$ mice treated with DMSO (vehicle), TB, anti-Ly6G, or TB plus anti-Ly6G (n = 5). (D–G) Overall survival of $APC^{min/+}$ mice treated with DMSO (vehicle), TB, anti-Ly6G, or TB plus anti-Ly6G. (E–G) IHC and statistical results of PCNA and Gr-1 staining in tumors derived from DMSO (vehicle)-, TB-, anti-Ly6G-, and TB plus anti-Ly6G-treated AOM/DSS mice. (H and I) $NADP^+$/NADPH ratio and G6PD activity in tumor cells resected from $APC^{min/+}$ mice. (J and K) Representative bioluminescence image and quantification of the total luminescence flux in mice bearing orthotopic xenografts and treated with DMSO (vehicle), TB, shSQLE, or TB plus shSQLE. (L and M) Tumor weight (n = 5) and overall survival curves (n = 10) of mice bearing orthotopic xenografts and treated with DMSO (vehicle), TB, shSQLE, or TB plus shSQLE. (N) G6PD activity in tumor cells resected from mice bearing orthotopic xenografts and treated as indicated (n = 5). (O) The proportion of MDSCs in orthotopic xenografts treated with DMSO (vehicle), TB, shSQLE, and TB plus shSQLE (n = 5). Data are presented as mean ± SD. (B, C, F–I, L, N, O) Unpaired two-tailed Student's t test. (D and M) Log rank test. (K) One-way ANOVA with Bonferroni correction. n.s., not significant; $p > 0.05$; $^*p < 0.05$; $^{**}p < 0.01$; and $^{***}p < 0.001$.

Please cite this article in press as: Hu et al., Terbinafine prevents colorectal cancer growth by inducing dNTP starvation and reducing immune suppression, Molecular Therapy (2022), https://doi.org/10.1016/j.ymthe.2022.06.015

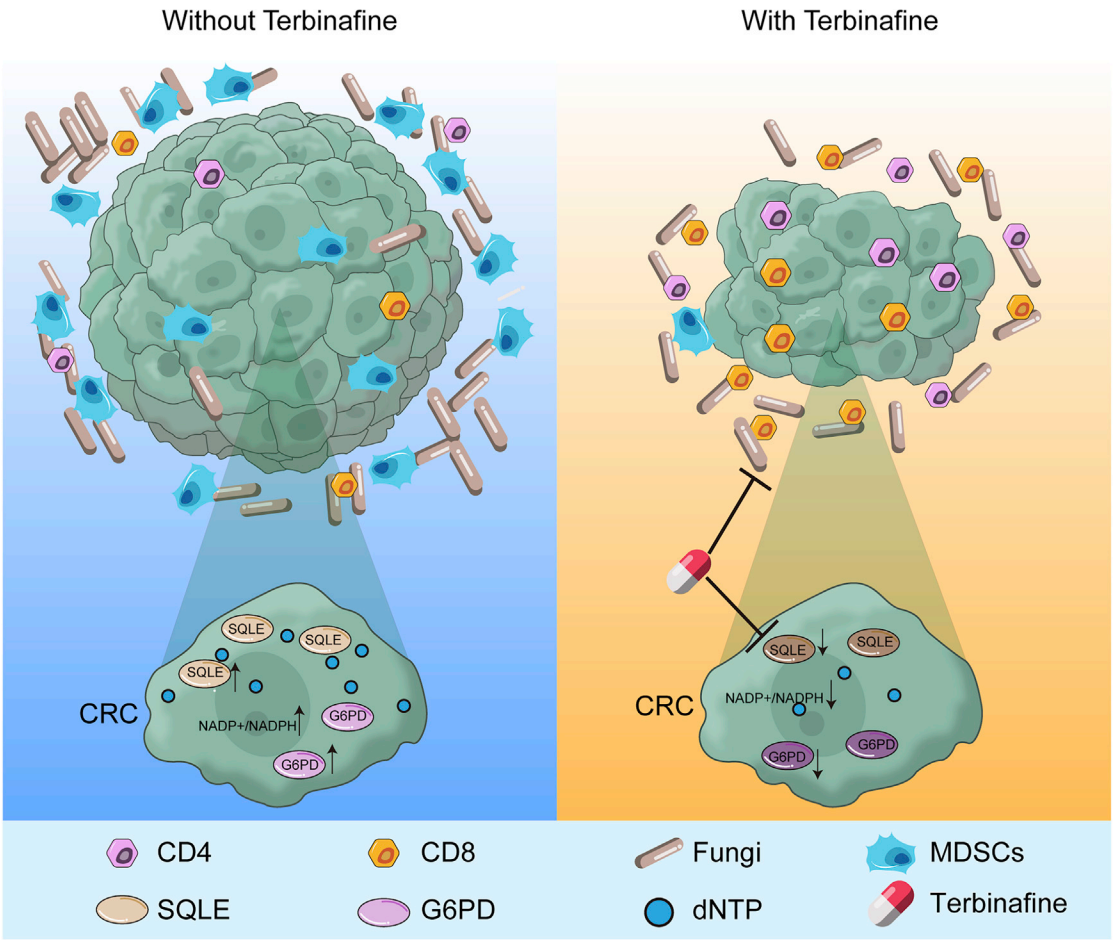

Figure 7. Proposed model for the antitumor effect of TB on CRC in mice

TB prevented CRC development through two mechanisms: inhibiting fungus-induced MDSC expansion and exerting direct cytotoxic effects on CRC cells, both evoking antitumor immune responses and suppressing cancer cell growth.

Cell-cycle assay

For the cell-cycle analysis, cells were serum starved for 12 h and treated with terbinafine for 24 h. The cells were then fixed in 75% ethanol overnight, stained with propidium iodide, and analyzed by flow cytometry. These experiments were conducted three times.

Colony formation assays

Briefly, 1,000 CRC cells suspended in 2 mL of McCoy's 5A medium were seeded into six-well plates after treatment under the indicated conditions. Culture medium was replaced every week. The cells were allowed to grow for the next 3 weeks to allow colony formation, and the colonies were visualized with crystal violet staining and quantified with ImageJ. These experiments were conducted three times.

Cell transfection and RNA interference

Plasmid transfection and small interfering RNA (siRNA) transfection were performed with Lipofectamine 2000 (Invitrogen, 11668019) and Lipofectamine RNAiMAX (Invitrogen, 13778150), respectively, following the manufacturer's instructions. C-terminal FLAG-tagged full-length cDNA encoding human SQLE was purchased from Genomeditech (Shanghai, China). Specific custom siRNAs were synthesized by GenePharma (Shanghai, China). For stable knockdown, shRNAs or sh scramble were cloned into the pLKO.1 plasmid (Sigma). The sequences of shRNA are listed in Table S4. Lentivirus packaging was performed in 293T cells according to standard protocols. Cells were infected with 1×10^6 recombinant lentivirus-transducing units in the presence of 10 mg/mL polybrene (Sigma, H9268). When grown to 40%–50% confluence, cells were infected with the indicated supernatant containing viral particles. Puromycin (Gibco, A1113802) was applied to virally infected cells to obtain stable knockdown or overexpression cell lines.

RNA isolation and gene expression study

Total RNA extraction and RNA reverse transcription were performed using TRIzol reagent (Takara, 9109) and PrimeScript RT-PCR kit (Takara, RR037A) according to standard protocols. SYBR Premix

Ex Taq (Roche, 04913914001) was used to run PCR on a 7500 Real-time PCR system (Applied Biosystems) at the recommended thermal settings. Relative mRNA expression was calculated using the $2^{(-\Delta\Delta Ct)}$ method and normalized to 18S mRNA levels. Primer sequences: *SQLE* (human) forward GGCATTGCCACTTTCACCTAT, reverse GGCCTGAGAGAATATCCGAGAAG; *Sqle* (mouse) forward AGTTCGCTGCCTTCTCGGATA, reverse GCTCCTGTTAATG TCGTTTCTGA; G6PD forward CGAGGCCGTCACCAAGAAC, reverse GTAGTGGTCGATGCGGTAGA; 18S forward TGCGAGT ACTCAACACCAACA, reverse GCATATCTTCGGCCCACA.

RNA sequencing

Total RNA of cell samples was isolated using TRIzol reagent for RNA sequencing following the manufacturer's instructions. Their qualities were checked using an Agilent 2100 Bioanalyzer (Agilent). The library fragments were purified with the AMPure XP system (Beckman Coulter, Beverly, USA). Clustering of the index-coded samples was performed on a cBot Cluster Generation System using TruSeq PE Cluster Kit v3-cBot-HS (Illumina) according to the manufacturer's instructions. After cluster generation, the library preparations were sequenced on an Illumina HiSeq X Ten, and 150-bp paired-end reads were generated. HTSeq v0.6.0 was used to count the read numbers mapped to each gene. The fragments per kilobase of exon model per million mapped fragments (FPKM) of each gene was then calculated based on the length of the gene and read count mapped to this gene.

Western blotting

The lysates of protein samples were collected by using WB Lysis and Extraction Buffer (Thermo Fisher, 89900), separated by SDS-PAGE in polyacrylamide gels, and transferred to nitrocellulose membranes. Subsequently, membranes were washed with 50-mM TRIS + 150-mM sodium chloride + 0.1% Tween 20, pH 7.4 (TBST) and blocked using 5% nonfat milk solution in TBST for at least 1 h at room temperature. Membranes were then incubated with primary antibodies: cleaved-caspase-8 (1:1,000, ImmunoWay, YC0011), cleaved-caspase-3 (1:1,000, ImmunoWay, YC0027), cleaved-caspase-7 (1:1,000, ImmunoWay, YC0010), cleaved-caspase-1 (1:1,000, ImmunoWay, YC0002), gasdermin D (1:1,000, CST, #46451), pMLKL (1:1,000, CST, #37333), MLKL (1:1,000, CST, #37705), β-actin (1:1,000, Abcam, ab8226). Molecular-weight-specific clipped bands were incubated with specific primary antibodies at 4°C overnight and were then incubated with horseradish peroxidase (HRP)-conjugated secondary antibodies (goat anti-mouse, 1:10,000, Jackson ImmunoResearch, 115-035-003; goat anti-rabbit, 1:10,000 Jackson ImmunoResearch, 111-035-003) for 1 h at room temperature. The primary and secondary antibodies were diluted in NCM Universal Antibody Diluent (New Cell & Molecular Biotech, WB500D).The bands were visualized with ECL reagents (ShareBio, SB-WB012).

Histology score

The histology score was performed by calculating the degree of both inflammation and dysplasia (0 = absence of inflammation and dysplasia, 1 = mild inflammation without significant dysplasia, 2 = moderate inflammation with no or mild dysplasia, 3 = severe inflammation with at most moderate dysplasia, 4 = severe inflammation with severe dysplasia). The final composite score was calculated by the sum of the scores from the middle and distal segment.

IHC

IHC was performed as previously described.[44] The proportion of PCNA-positive cells was determined by counting immunostain-positive cells as a percentage of the total number of nuclei in the field. COX2 and immune cells (CD4, CD8, and Gr-1) quantification were calculated based on pixel intensity. IHC quantification was conducted independently by two senior pathologists in a blinded manner. All antibodies were diluted with PBS (B320KJ, BasalMedia) containing 1% BSA Albumin Fraction V (4240GR250, BioFroxx). The primary antibodies used for IHC were PCNA (1:500, CST, 13110), COX2 (1:100, Abcam, ab179800), Gr-1 (1:100, Invitrogen Antibodies, 14-5931-82), CD8 (1:100, Cell Signaling, 98941), CD4 (1:1,00, Cell Signaling, 25229), and SQLE (1:100, Proteintech, 12544-1-AP). After washing thrice, slides were developed in DAB (CST, 8059) for an appropriate time and counterstained with hematoxylin.

Liquid chromatography-mass spectrometry analysis of cell metabolites

Cells with various treatments were cultured with McCoy's 5A, half of which were U-^{13}C labeled (CIL, CLM-1396-1) for 1 h. The cells (5×10^6) were washed twice with cold PBS. After centrifugation, ice-cold extraction buffer (methanol:acetonitrile:H_2O = 2:2:1) was immediately added to the cell pellets at five volumes. Samples were treated with freeze and thaw cycles (freeze in liquid nitrogen for 1 min and thaw at room temperature) at least three times to lyse cells sufficiently. The same volume of chloroform was then added to the samples and vortexed for 10 s. Mixtures were centrifuged at 12,000 rpm for 15 min, and the supernatant was collected and dried. The powder-containing metabolites were dissolved in 80% methanol to run liquid chromatography-mass spectrometry (LC-MS).

Flow cytometry

Mice were euthanized and colons were harvested. Colon tissues were carefully minced and digested by digestion buffer (1 mg/mL collagenase IV) for 1 h at 37°C under slow rotation, then the leukocyte populations were enriched by 37.5% Percoll gradient. The cells were washed and finally resuspended in the staining buffer (2% FBS in PBS). Single-cell suspensions were incubated with fluorochrome-conjugated antibodies at recommended dilutions or with isotype control antibodies listed above for 20 min at 4°C. 7-AAD was used to determine the living status of immune cells. Stained cells were analyzed by flow cytometry (LSRFortessa, Becton Dickinson). CD45 (12-0451-82, eBioscience), 7-AAD (00-6993-50, eBioscience), CD11b (17-0112-82, BD Pharmingen), Gr1 antibody (108412, Biolegend), CD3 (100308, Biolegend), CD4 (11-0042-82, eBioscience), and CD8 (17-0081-82, eBioscience). FlowJo v.10.4.2 was used for further analysis.

$NADP^+$/NAPDH ratio

Cells (2×10^6) or tissues (50 mg) were harvested and lysed to determine the intracellular $NADP^+$/NAPDH ratio by using cell lysates

according to the manufacturer's instructions (Biovision, #K347). The values were normalized to the protein concentration. This experiment was conducted three times.

G6PD enzyme activity

Cells (2×10^6) or tissues (50 mg) were harvested and lysed to quantify G6PD enzyme activity with a PicoProbe Glucose-6-Phosphate Dehydrogenase Activity Assay Kit (Fluorometric) (Biovision, #K751). The values were normalized based on protein concentration, which was determined by a BCA Assay Kit (Pierce). This experiment was conducted three times.

Fecal fungal loading

The total fungal load in mouse feces was determined by using quantitative PCR. Mouse fecal DNA was extracted from stools and quantified by TaqMan qPCR using the primers Fungi-quant-F 5′-GGRAAACTCACCAGGTCCAG-3′ and Fungi-quant-R 5′-GSWCTATCCCCAKCACGA-3′ and the probe 5′-TGGTGCATGGCCGTT-3′.

Fungal sequencing and analysis

DNA was isolated from the feces of mice as described above. Fungal diversity was determined by ITS sequencing. The sequencing was performed using a Gs-FLX Titanium Sequencing System (Roche, Mannheim, Germany). The sequences were assigned to OTUs using the USEARCH (version 10.0) algorithm. PCAs based on fungal composition were performed.

DATA AVAILABILITY

The datasets of CRC cell lines treated with terbinafine that support the findings of this study are available in the Sequence Read Archive (SRA) repository under accession number SUB7214368. All other remaining data that support the findings of this study are available from the authors upon reasonable request.

SUPPLEMENTAL INFORMATION

Supplemental information can be found online at https://doi.org/10.1016/j.ymthe.2022.06.015.

ACKNOWLEDGMENTS

This work was supported by grants awarded L.-P.H. from the National Natural Science Foundation of China (82103357), Shanghai Sailing Program (21YF1445200), Natural Science Foundation of Shanghai (21ZR1461300) and to J.J. by the Swedish Research Council (2021-01187), Cancerfonden (CAN2017/340), and MAS Cancer, to Z.-G.Z. by the National Natural Science Foundation of China (92168111), the Shanghai Municipal Education Commission-Gaofeng Clinical Medicine Grant Support (20181708), Program of Shanghai Academic/Technology Research Leader (19XD1403400), Medicine and Engineering Interdisciplinary Research Fund of Shanghai Jiao Tong University (YG2021ZD08), Innovative research team of high-level local universities in Shanghai (SHSMU-ZDCX20210802), to J.L.; the National Natural Science Foundation of China (82073023, 81871923), the Shanghai Municipal Education Commission-Gaofeng Clinical Medicine Grant Support (ID 20191809), to X.W.; the National Natural Science Foundation of China (32170910), the Natural Science Foundation of Jiangsu Province (BK20211124), Zhenjiang Key Research and Development Program (SH2021037), to J.S. by the National Natural Science Foundation of China (31970745). The funding agencies had no role in the design and conduct of the study; in the collection, analysis, and interpretation of the data; or in the preparation, review, or approval of the manuscript. The researchers were independent of the funding agencies.

AUTHOR CONTRIBUTIONS

Conceptualization, L.-P.H., Z.-G.Z., and J.J.; methodology, L.-P.H., W.H., X.W., C.X., W.-T.Q., D.X.L., G.T., Q.L., Y.Z., and S.C; investigation, L.-P.H., Z.-G.Z., J.J., H.-Z.N., Y.H., J.S., and X.-L.Z.; formal analysis, L.-P.H., W.H., J.L., and S.-H.J.; writing, L.-P.H., Z.-G.Z., and J.J.; supervision, J.J., Z.-G.Z., J.S., and K.S.. All authors revised the article for important intellectual content.

DECLARATION OF INTERESTS

The authors declare no competing interests.

REFERENCES

1. Bray, F., Ferlay, J., Soerjomataram, I., Siegel, R.L., Torre, L.A., and Jemal, A. (2018). Global cancer statistics 2018: GLOBOCAN estimates of incidence and mortality worldwide for 36 cancers in 185 countries. CA Cancer J. Clin. *68*, 394–424. https://doi.org/10.3322/caac.21492.
2. Dušek, L., Mužík, J., Malúšková, D., and Šnajdrová, L. (2014). Epidemiology of colorectal cancer: international comparison. In Institute of Biostatistics and Analyses (Masaryk University).
3. Siegel, R.L., Miller, K.D., and Jemal, A. (2020). Cancer statistics. CA Cancer J. Clin. *70*, 7–30. https://doi.org/10.3322/caac.21590.
4. Kamada, N., Seo, S.-U., Chen, G.Y., and Núñez, G. (2013). Role of the gut microbiota in immunity and inflammatory disease. Nat. Rev. Immunol. *13*, 321–335. https://doi.org/10.1038/nri3430.
5. Lavelle, A., and Sokol, H. (2020). Gut microbiota-derived metabolites as key actors in inflammatory bowel disease. Nat. Rev. Gastroenterol. Hepatol. *17*, 223–237. https://doi.org/10.1038/s41575-019-0258-z.
6. Wong, S.H., and Yu, J. (2019). Gut microbiota in colorectal cancer: mechanisms of action and clinical applications. Nat. Rev. Gastroenterol. Hepatol. *16*, 690–704. https://doi.org/10.1038/s41575-019-0209-8.
7. Yu, T., Guo, F., Yu, Y., Sun, T., Ma, D., Han, J., Qian, Y., Kryczek, I., Sun, D., Nagarsheth, N., et al. (2017). Fusobacterium nucleatum promotes chemoresistance to colorectal cancer by modulating autophagy. Cell *170*, 548–563.e16. https://doi.org/10.1016/j.cell.2017.07.008.
8. Tilg, H., Adolph, T.E., Gerner, R.R., and Moschen, A.R. (2018). The intestinal microbiota in colorectal cancer. Cancer Cell *33*, 954–964. https://doi.org/10.1016/j.ccell.2018.03.004.
9. Coker, O.O., Nakatsu, G., Dai, R.Z., Wu, W.K.K., Wong, S.H., Ng, S.C., Chan, F.K.L., Sung, J.J.Y., and Yu, J. (2019). Enteric fungal microbiota dysbiosis and ecological alterations in colorectal cancer. Gut *68*, 654–662. https://doi.org/10.1136/gutjnl-2018-317178.
10. Sokol, H., Leducq, V., Aschard, H., Pham, H.-P., Jegou, S., Landman, C., Cohen, D., Liguori, G., Bourrier, A., Nion-Larmurier, I., et al. (2017). Fungal microbiota dysbiosis in IBD. Gut *66*, 1039–1048. https://doi.org/10.1136/gutjnl-2015-310746.
11. Malik, A., Sharma, D., Malireddi, R.S., Guy, C.S., Chang, T.-C., Olsen, S.R., Neale, G., Vogel, P., and Kanneganti, T.D. (2018). SYK-CARD9 signaling axis promotes gut fungi-mediated inflammasome activation to restrict colitis and colon cancer. Immunity *49*, 515–530.e5. https://doi.org/10.1016/j.immuni.2018.08.024.

12. Motamedian, E., Taheri, E., and Bagheri, F. (2017). Proliferation inhibition of cisplatin-resistant ovarian cancer cells using drugs screened by integrating a metabolic model and transcriptomic data. Cell Prolif. *50*, e12370. https://doi.org/10.1111/cpr.12370.

13. Lee, W.S., Chen, R.J., Wang, Y.J., Tseng, H., Jeng, J.H., Lin, S.Y., Liang, Y.C., Chen, C.H., Lin, C.H., Lin, J.K., et al. (2003). In vitro and in vivo studies of the anticancer action of terbinafine in human cancer cell lines: G0/G1 p53-associated cell cycle arrest. Int. J. Cancer *106*, 125–137. https://doi.org/10.1002/ijc.11194.

14. Maione, F., Oliaro-Bosso, S., Meda, C., Di Nicolantonio, F., Bussolino, F., Balliano, G., Viola, F., and Giraudo, E. (2015). The cholesterol biosynthesis enzyme oxidosqualene cyclase is a new target to impair tumour angiogenesis and metastasis dissemination. Sci. Rep. *5*, 9054. https://doi.org/10.1038/srep09054.

15. Liu, D., Wong, C.C., Fu, L., Chen, H., Zhao, L., Li, C., Zhou, Y., Zhang, Y., Xu, W., Yang, Y., et al. (2018). Squalene epoxidase drives NAFLD-induced hepatocellular carcinoma and is a pharmaceutical target. Sci. Transl. Med. *10*, eaap9840. https://doi.org/10.1126/scitranslmed.aap9840.

16. Neufert, C., Becker, C., and Neurath, M.F. (2007). An inducible mouse model of colon carcinogenesis for the analysis of sporadic and inflammation-driven tumor progression. Nat. Protoc. *2*, 1998–2004. https://doi.org/10.1038/nprot.2007.279.

17. Zigmond, E., Halpern, Z., Elinav, E., Brazowski, E., Jung, S., and Varol, C. (2011). Utilization of murine colonoscopy for orthotopic implantation of colorectal cancer. PLoS One *6*, e28858. https://doi.org/10.1371/journal.pone.0028858.

18. Karki, R., Sharma, B.R., Lee, E., Banoth, B., Malireddi, R.S., Samir, P., Tuladhar, S., Mummareddy, H., Burton, A.R., Vogel, P., and Kanneganti, T.D. (2020). Interferon regulatory factor 1 regulates PANoptosis to prevent colorectal cancer. JCI Insight *5*, 136720. https://doi.org/10.1172/jci.insight.136720.

19. Wang, T., Fan, C., Yao, A., Xu, X., Zheng, G., You, Y., Jiang, C., Zhao, X., Hou, Y., Hung, M.C., and Lin, X. (2018). The adaptor protein CARD9 protects against colon cancer by restricting mycobiota-mediated expansion of myeloid-derived suppressor cells. Immunity *49*, 504–514.e4. https://doi.org/10.1016/j.immuni.2018.08.018.

20. Malínsky, J., Koberna, K., Stanek, D., Masata, M., Votruba, I., and Raska, I. (2001). The supply of exogenous deoxyribonucleotides accelerates the speed of the replication fork in early S-phase. J. Cell Sci. *114*, 747–750. https://doi.org/10.1242/jcs.114.4.747.

21. Patra, K.C., and Hay, N. (2014). The pentose phosphate pathway and cancer. Trends Biochem. Sci. *39*, 347–354. https://doi.org/10.1016/j.tibs.2014.06.005.

22. Kimura, K., Spate, L.D., Green, M.P., and Roberts, R.M. (2005). Effects of D-glucose concentration, D-fructose, and inhibitors of enzymes of the pentose phosphate pathway on the development and sex ratio of bovine blastocysts. Mol. Reprod. Dev. *72*, 201–207. https://doi.org/10.1002/mrd.20342.

23. Ochi, R., Chettimada, S., Kizub, I., and Gupte, S.A. (2018). Dehydroepiandrosterone inhibits ICa, L and its window current in voltage-dependent and -independent mechanisms in arterial smooth muscle cells. Am. J. Physiol. Heart Circ. Physiol. *315*, H1602–H1613. https://doi.org/10.1152/ajpheart.00291.2018.

24. Helmink, B.A., Khan, M.A.W., Hermann, A., Gopalakrishnan, V., and Wargo, J.A. (2019). The microbiome, cancer, and cancer therapy. Nat. Med. *25*, 377–388. https://doi.org/10.1038/s41591-019-0377-7.

25. Pleguezuelos-Manzano, C., Puschhof, J., Huber, A.R., and van Hoeck, A. (2020). Mutational signature in colorectal cancer caused by genotoxic pks(+) E. coli. Nature *580*, 269–273.

26. Aykut, B., Pushalkar, S., Chen, R., Li, Q., Abengozar, R., Kim, J.I., Shadaloey, S.A., Wu, D., Preiss, P., Verma, N., et al. (2019). The fungal mycobiome promotes pancreatic oncogenesis via activation of MBL. Nature *574*, 264–267. https://doi.org/10.1038/s41586-019-1608-2.

27. Kumar, V., Patel, S., Tcyganov, E., and Gabrilovich, D.I. (2016). The nature of myeloid-derived suppressor cells in the tumor microenvironment. Trends Immunol. *37*, 208–220. https://doi.org/10.1016/j.it.2016.01.004.

28. Talmadge, J.E., and Gabrilovich, D.I. (2013). History of myeloid-derived suppressor cells. Nat. Rev. Cancer *13*, 739–752. https://doi.org/10.1038/nrc3581.

29. Rieber, N., Singh, A., Oz, H., Carevic, M., Bouzani, M., Amich, J., Ost, M., Ye, Z., Ballbach, M., Schäfer, I., et al. (2015). Pathogenic fungi regulate immunity by inducing neutrophilic myeloid-derived suppressor cells. Cell Host Microbe *17*, 507–514. https://doi.org/10.1016/j.chom.2015.02.007.

30. Maxfield, L., Preuss, C.V., and Bermudez, R. (2019). Terbinafine. Drugs *43*, 259–284.

31. Lemke, A., Kiderlen, A.F., and Kayser, O. (2005). Amphotericin B. Appl. Microbiol. Biotechnol. *68*, 151–162. https://doi.org/10.1007/s00253-005-1955-9.

32. Agrawal, P.B., Narang, A., and Kumar, P. (1996). Fluconazole. Indian J. Pediatr. *63*, 775–780. https://doi.org/10.1007/bf02730928.

33. Fernández, M.S., Rojas, F.D., Cattana, M.E., Sosa, M. d l Á., Iovannitti, C.A., Lass-Flörl, C., and Giusiano, G.E. (2015). In vitro activities of amphotericin B, terbinafine, and azole drugs against clinical and environmental isolates of Aspergillus terreus sensu stricto. Antimicrob. Agents Chemother. *59*, 3619–3622. https://doi.org/10.1128/aac.00045-15.

34. Gülmez, D., Doğan, Ö., Boral, B., Döğen, A., Ilkit, M., de Hoog, G.S., and Arikan-Akdagli, S. (2018). In vitro activities of antifungal drugs against environmental Exophiala isolates and review of the literature. Mycoses *61*, 561–569. https://doi.org/10.1111/myc.12779.

35. Brown, D.N., Caffa, I., Cirmena, G., Piras, D., Garuti, A., Gallo, M., Alberti, S., Nencioni, A., Ballestrero, A., and Zoppoli, G. (2016). Squalene epoxidase is a bona fide oncogene by amplification with clinical relevance in breast cancer. Sci. Rep. *6*, 19435. https://doi.org/10.1038/srep19435.

36. Howe, V., Sharpe, L.J., Prabhu, A.V., and Brown, A.J. (2017). New insights into cellular cholesterol acquisition: promoter analysis of human HMGCR and SQLE, two key control enzymes in cholesterol synthesis. Biochim. Biophys. Acta Mol. Cell Biol. Lipids *1862*, 647–657. https://doi.org/10.1016/j.bbalip.2017.03.009.

37. Stopsack, K.H., Gerke, T.A., Sinnott, J.A., Penney, K.L., Tyekucheva, S., Sesso, H.D., Andersson, S.O., Andrén, O., Cerhan, J.R., Giovannucci, E.L., et al. (2016). Cholesterol metabolism and prostate cancer lethality. Cancer Res. *76*, 4785–4790. https://doi.org/10.1158/0008-5472.can-16-0903.

38. Brown, A.J., Chua, N.K., and Yan, N. (2019). The shape of human squalene epoxidase expands the arsenal against cancer. Nat. Commun. *10*, 888. https://doi.org/10.1038/s41467-019-08866-y.

39. Mahoney, C.E., Pirman, D., Chubukov, V., Sleger, T., and Hayes, S. (2019). A chemical biology screen identifies a vulnerability of neuroendocrine cancer cells to SQLE inhibition. Nat. Commun. *10*, 96.

40. Punt, C.J.A., Koopman, M., and Vermeulen, L. (2017). From tumour heterogeneity to advances in precision treatment of colorectal cancer. Nat. Rev. Clin. Oncol. *14*, 235–246. https://doi.org/10.1038/nrclinonc.2016.171.

41. Huang, W., Sundquist, J., Sundquist, K., and Ji, J. (2020). Phosphodiesterase-5 inhibitors use and risk for mortality and metastases among male patients with colorectal cancer. Nat. Commun. *11*, 3191. https://doi.org/10.1038/s41467-020-17028-4.

42. Zhang, N., Sundquist, J., Sundquist, K., and Ji, J. (2020). An increasing trend in the prevalence of polypharmacy in Sweden: a nationwide register-based study. Front Pharmacol. *11*, 326. https://doi.org/10.3389/fphar.2020.00326.

43. Ji, J., Sundquist, J., and Sundquist, K. (2019). Use of terbinafine and risk of death in patients with prostate cancer: a population-based cohort study. Int. J. Cancer *144*, 1888–1895. https://doi.org/10.1002/ijc.31901.

44. Hu, L.P., Zhou, K.X., Huo, Y.M., Liu, D.J., Li, Q., Yang, M.W., Huang, P.Q., Xu, C.J., Tian, G.A., Yao, L.L., et al. (2021). Single-cell RNA sequencing reveals that targeting HSP90 suppresses PDAC progression by restraining mitochondrial bioenergetics. Oncogenesis *10*, 22. https://doi.org/10.1038/s41389-021-00311-4.